Engineering 26 (2023) 220–228

Contents lists available at ScienceDirect

Engineering

journal homepage: www.elsevier.com/locate/eng

Research
Environmental Engineering—Article

One-Step Synthesis of Structurally Stable CO_2-Philic Membranes with Ultra-High PEO Loading for Enhanced Carbon Capture

Bin Zhu [a], Shanshan He [a], Yadong Wu [a], Songwei Li [b], Lu Shao [a,*]

[a] MIIT Key Laboratory of Critical Materials Technology for New Energy Conversion and Storage, State Key Laboratory of Urban Water Resource and Environment, School of Chemistry and Chemical, Harbin Institute of Technology, Harbin 150001, China
[b] Key Laboratory of Materials Processing and Mold (Zhengzhou University), Ministry of Education, National Engineering Research Center for Advanced Polymer Processing Technology Department of Chemical Engineering, Zhengzhou University, Zhengzhou 450002, China

ARTICLE INFO

Article history:
Received 3 November 2021
Revised 10 March 2022
Accepted 21 March 2022
Available online 12 May 2022

Keywords:
Membrane separation
Gas separation
CO_2 capture
CO_2-philic membrane
Poly(ethylene oxide)

ABSTRACT

Membrane technology has been considered a promising strategy for carbon capture to mitigate the effects of increasing atmospheric CO_2 levels because CO_2-philic membranes have demonstrated significant application potential, especially, for CO_2/light gas separation. In this regard, poly(ethylene oxide) (PEO), which is a representative CO_2-philic material, has attracted extensive research attention owing to its specific dipole–quadrupole interaction with CO_2. Herein, we report a facile one-step synthesis protocol via the *in situ* polymerization of highly flexible polyethylene glycol to overcome the limitations of PEO, including high crystallinity and poor mechanical strength. The robust structure derived from intricate entanglements between short PEO chains and the polymer matrix enables an extremely high loading of linear polyethylene glycol (up to 90 wt%). Consequently, the separation performance easily surpasses the upper-bound limit. Moreover, the high structural stability allows for the concurrent increase of CO_2 permeability and CO_2/light gas selectivity at high feed pressure (up to 20 bar (1 bar = 10^5 Pa)). This study provides a promising strategy to simultaneously improve the toughness and gas separation properties of all-polymeric membranes, demonstrating significant potential for industrial carbon capture and gas purification.

1. Introduction

Climate change, induced by steadily increasing CO_2 emission since the 1900s, has emerged as a global challenge. There is an urgent need to adopt active measures to mitigate carbon emission [1–3]. The European Commission has identified carbon capture and storage as a key decarbonization option for the electricity sector and energy-intensive industries and has also pledged the achievement of carbon neutrality by 2050. Furthermore, the net worth of global carbon capture and storage market is expected to reach 6.13×10^9 USD per annum by 2027 [4–6]. Therefore, developing superior separation technologies to capture or purify exhaust gases is necessary to sustain national prosperity. In this regard, membrane technology has emerged as a promising alternative to CO_2 capture because of its high energy efficiency, low footprint, and modifiable operation process [7–9]. Particularly, CO_2-philic membranes, fabricated with poly(ethylene oxide) (PEO) and its derivatives, have been widely studied for their strong dipole–quadrupole interactions with CO_2 molecules [10,11]. However, the trade-off between permeability and selectivity significantly hinders the separation performance of traditional PEO-containing polymers and limits their extensive application in industrial processes [12]. Consequently, it is necessary to further explore the potential of PEO-based materials.

The conventional strategy to address this trade-off is via the preparation of mixed matrix membranes (MMMs), which consist of two parts: a processable polymer matrix and highly efficient inorganic particles (as fillers) [13,14]. However, the combination of organic and inorganic materials easily leads to the uneven dispersion of fillers and undesirable defects between polymer matrix and inorganic materials [15–17]. Considering the uncertain compatibility between polymers and fillers, to overcome the limitations of MMMs, polymer blending has been adopted owing to its convenience, implementation ability, and commercial potential [18–21]. Low molecular weight PEOs (LMWPEO) are a class of

* Corresponding author.
E-mail address: shaolu@hit.edu.cn (L. Shao).

https://doi.org/10.1016/j.eng.2022.03.016

highly efficient additives, which not only allows mutual miscibility with PEO-based materials but also improves polymer flexibility, optimizes fractional free volumes (FFVs), and eventually promotes gas transport [22,23]. Yave et al. [24] reported that when polyethylene glycol dimethyl ether (PEGDME) was employed as an additive to the Pebax matrix, the phase separation of PEO and polyamide 6 (PA6) was enhanced by the alkyl groups on PEGDME. This resulted in a larger number of PEO chain segments forming microdomains that were more conducive to CO_2 transport. Moreover, the glass transition temperature (T_g) of the polymer was reduced from 220 to 195 K, providing further evidence of improved chain segment motility. Therefore, the CO_2 permeability of the Pebax-PEGDME membrane is much higher than that of the pristine Pebax membrane. Furthermore, our group was the first to demonstrate that the gas transport performance of cross-linked PEO membranes can be improved via a facile impregnation method [25]. FFVs of the cross-linked PEO films consistently increased with the PEG amount, owing to the plasticization effect. Additionally, the immersed PEG significantly enhanced the CO_2 solubility of the membrane as a function of its high ethylene oxide (EO) content.

However, embedded LMWPEOs cause structural instability. The mechanical strength of a membrane primarily relies on the entanglement and crystal of polymeric chains [26,27]. Short linear PEO molecules weaken the interactions among adjacent chains. Therefore, the amount of additives that can be used is significantly limited because of the deterioration of mechanical property of the membrane, hindering further improvement of its separation performance. What's more, LMWPEOs are also easily extruded at high operating pressures, damaging the membrane structure and causing separation performance degradation, which limits their application under harsh conditions. Hence, addressing this trade-off between mechanical property and separation efficiency is of critical urgency.

Herein, we propose a one-step method that incorporates poly(ethylene glycol) methyl ether acrylate (PEGMEA) with high EO content into the Pebax matrix. The *in situ* polymerization of vinyl-functionalized PEGMEA monomers can be initiated via thermal treatment, while the methyl termination of the side chains can create an open structure for the ease of transport. The resulting highly branched poly-PEGMEA helps generate sufficient entanglement with polymer chains to guarantee adequate mechanical strength even under massive loading. This self-polymerized membrane is expected to subtly synergize the robust physical structure with the gas separation performance, unlike a simply blended Pebax/PEGMEA membrane. We believe this study will open a pathway for the rational design of ultra-stable membranes under harsh conditions.

2. Experimental procedures

2.1. Materials

Pebax® MH 1657 (Pebax) was obtained from Arkema Co., Ltd. (France). PEGMEA (number-average molecular weight (M_n) = 480) and 2,2′-azobis (2-methylpropionitrile) (AIBN) were obtained from Sigma-Aldrich Co., LLC (USA). Anhydrous ethanol (AR) was supplied by Tianjin Kemao Chemical Reagent Co., Ltd. (China). Deionized water (DI) was used throughout the study.

2.2. Preparation of the membranes

A specified quantity of Pebax was dissolved in a mixture of 70 wt% ethanol and 30 wt% water. Thereafter, the obtained mixture was refluxed for 2 h at 80 °C to acquire 3 wt% Pebax homogeneous solution. After cooling to ambient temperature, the solution was cast on a homemade glass mold, dried in air for 48 h, and then heated in a vacuum oven at 40 °C to ensure complete solvent evaporation. A self-polymerization-confined membrane was fabricated by uniformly mixing PEGMEA in a Pebax solution, while AIBN (1 wt%) was simultaneously added as an initiator. After solvent evaporation, the glass mold was heated to 80 °C in a vacuum oven for 2 h to ensure sufficient polymerization. For the ease of differentiation, the resulting self-polymerized membranes were denoted as SPM-*A*, and the membrane without further thermal treatment was denoted as PMEA-*B*, where *A* and *B* are the mass fractions of PEGMEA. The mass fraction (w_f) was calculated using Eq. (1):

$$w_f = \frac{m_1}{m_1 + m_2} \times 100\% \quad (1)$$

where m_1 and m_2 represent the masses of PEGMEA and Pebax matrix, respectively.

2.3. Characterization

Attenuated total reflectance Fourier transform infrared (ATR-FTIR) spectra were obtained using a PerkinElmer Spectrum Two (USA) at ambient temperature from 4000 to 500 cm^{-1}. Packing motifs of polymer chains were measured using wide-angle X-ray diffraction (WAXD) on a Bruker D8 ADVANCE X-ray diffractometer (40 kV, 40 mA, Cu Kα, λ = 1.5418 Å; Germany) in a 5°–80° range with a scan speed of 5°·min^{-1} at room temperature. X-ray photoelectron spectroscopy (XPS) was conducted on a Thermo ESCALAB 250XI (Al Kα, $h\nu$ = 1486.6 eV; Thermo Scientific, USA) at room temperature. Differential scanning calorimetry (DSC; Q200, TA) was used to study thermal properties. Initial heating was performed at a heating rate of 20 °C·min^{-1} to eliminate the heating history. The exothermic curves of the membranes were recorded from −90 to 250 °C at a scanning rate of 10 °C·min^{-1} under a N_2 atmosphere. The area swelling and water uptake of the membranes were determined by soaking the dry film (cut into 2 cm diameter round pieces) in water for 72 h. Water was changed every 12 h. The ratio of the area difference between the dry and wet films to that of the dry membrane corresponds to the area swelling of the films. Water uptake was calculated in the same manner. Weight loss was measured as the ratio of the weight difference between the membranes before and after water absorption to the dry membrane before water was absorbed. The membranes were trimmed into 4 cm × 1 cm pieces for tensile testing (tensile testing machine was CTM2050; Xie Qiang, China), and the stretching velocity was set at 5 mm·min^{-1}. The membrane thickness was measured using a micrometer caliper, and each membrane was measured nine times to obtain an average value. Small-angle X-ray scattering (SAXS) was performed via Saxesess mc2 (Anton Paar, Germany) using Kα radiation from 0.08° to 5° at room temperature. The thermal stability of membranes was tested using a thermogravimetric analyzer (TGA; Q500, TA) at a heating rate of 10 °C·min^{-1} from 20 to 800 °C under a N_2 atmosphere. Polymer density was determined via the buoyancy method using a Mettler Toledo balance (ME104; Switzerland) and density determination kit. The membrane density (ρ_m) was calculated as follows:

$$\rho_m = \frac{m_a}{m_a - m_b}\rho_0 \quad (2)$$

where m_a and m_b represent membrane weights in air and auxiliary liquids, respectively. ρ_0 is the density of the silicone oil auxiliary liquid (0.968 g·cm^{-3}).

2.4. Gas permeation test

Gas permeation was analyzed using a homemade apparatus employing the constant volume/variable pressure method.

Following our previous study, gas permeation was tested in the following order: $H_2 \rightarrow N_2 \rightarrow CO_2$ [28]. The gas pressure was maintained at 3.5 bar (1 bar = 10^5 Pa), and the test temperature was controlled at 35 °C, unless specified otherwise. Detailed information on gas testing is provided in Appendix A.

3. Results and discussion

SPM membranes were obtained by introducing PEGMEA in the Pebax solution, followed by *in situ* polymerization during thermal treatment (Fig. 1). Poly-PEGMEA exhibits a highly branched structure, which is capable of dynamic entanglement with polymer chains. For the PMEA membrane, the chain length of the low molar weight PEGMEA is very short to form an effective entanglement. Therefore, the maximum PEGMEA loading of the PMEA membrane was 70 wt%, while it was up to 90 wt% for SPM membranes, which represents the state-of-the-art in similar membrane materials.

3.1. Stability of self-polymerized structure

To confirm the construction and reliability of the self-polymerized structure, we measured the weight loss, water uptake, and area swelling of the SPM and PMEA membranes by soaking them in pure water for 72 h (Figs. 2(a) and (b); Figs. S1 and S2 in Appendix A). As shown in Fig. 2(a), almost all SPM membranes exhibited a gel content of more than 80% in water, demonstrating that the linear PEGMEA was successfully polymerized and the resulting poly-PEGMEA intertwined strongly with Pebax chains. In contrast, the weight loss of the PMEA membranes increased with PEGMEA loading, which proved that most of the PEGMEA content dissolved out from the membranes. The opposite trend in water absorption reflected the loss of the EO content in the PMEA membrane, whereas the SPM-90 membrane showed approximately three times larger absorption capability than the Pebax membrane. This is because of the introduction of a large number of hydrophilic EO groups. Similarly, the distinct difference in the area swelling (Figs. S1 and S2) also indicated the formation of a new stable structure that endows the membrane with high stability.

Mechanical properties of the membrane are represented by the stress–strain curves shown in Figs. 2(c) and (d) and Fig. S3 in Appendix A. The incremental embedding of PEGMEA deteriorates the mechanical strength of the Pebax matrix owing to the plasticization effect. On the contrary, the SPM membranes exhibit a higher performance than the PMEA membranes in terms of both breaking strength and maximum elongation, confirming that the thermal treatment successfully intertwined Pebax chains and branched poly-PEGMEA. This dynamic entanglement facilitates a firm interlocking in the self-polymerized structure to reinforce the polymer chains and prevent the membrane from breaking. In other words, self-polymerization-confined membranes show better mechanical stability than conventional LMWPEO composite materials, making the membranes suitable for a wider range of industrial applications.

3.2. Structure characterization of SPM membranes

Chemical structures of the SPM membranes were analyzed using XPS and ATR-FTIR. According to the XPS results (Fig. 3(a); Fig. S4 and Table S1 in Appendix A), the disappearance of the C–N peak at 286.05 eV and the diminution of N atom percentage confirm the introduction of PEGMEA. The peak at 283.3 eV in the C 1s spectrum of SPM-90 corresponds to aliphatic chains, confirming the formation of poly-PEGMEA [29–31]. In the ATR-FTIR spectra of Pebax (Fig. S5 in Appendix A), the absorption intensity of the amide N–H (3299 cm^{-1}) and amide carbonyl H–N–C=O (1640 cm^{-1}) groups decreased. On the contrary, the absorption intensity of C=O groups (1730 cm^{-1}) in both Pebax and PEGMEA increased with the addition of PEGMEA [27,32,33]. The strongest adsorption bond at approximately 1100 cm^{-1} denotes the asymmetrical stretching vibration of C–O–C units [34]. No significant band shift was observed between the different Fourier transform infrared (FT-IR) spectra, indicating a similar chemical structure and good compatibility of these two polymers, which is beneficial for the construction of a homogeneous membrane.

The FFV of a polymer is related to its density. Herein, we measured the membrane density with different PEGMEA volume fractions and compared them with the results of the additive model, as shown in Fig. 3(b). The additive model is defined by the following Eq. (3):

$$\rho = \Phi_1\rho_1 + (1 - \Phi_1)\rho_2 \tag{3}$$

where Φ_1 is the Pebax volume fraction, which can be estimated using the experimental density. ρ_1 is the Pebax density, and ρ_2 represents the density of PEGMEA and poly-PEGMEA in the PMEA and SPM membranes, respectively. The density of poly-PEGMEA was adopted from the Freeman's study [35]. Notably, the density of the composite membrane merely relies on the polymer component of the system, according to Eq. (3). Therefore, the distinction in density between the experimental data and theoretical values may exist owing to the structural variation of the polymer (i.e., variation of FFV).

As shown in Fig. 3(b), the values for SPM membranes are higher than those for PMEA membranes, indicating the self-polymerization of PEGMEA in SPM membranes, which is in agreement with XPS results. In addition, the experimental densities of both SPM and PMEA membranes were lower than those obtained using the additive model. Specifically, when the volume fraction of PEGMEA is less than 50%, the density of the SPM membrane is even less than that of the PMEA membrane obtained using the additive model. This proves that poly-PEGMEA can effectively disturb the polymer structure of Pebax. Pebax is a typical copolymer consisting of a PEO and PA6 segments, and a distinct hydrogen bond interaction exists between the amide bond and the EO unit.

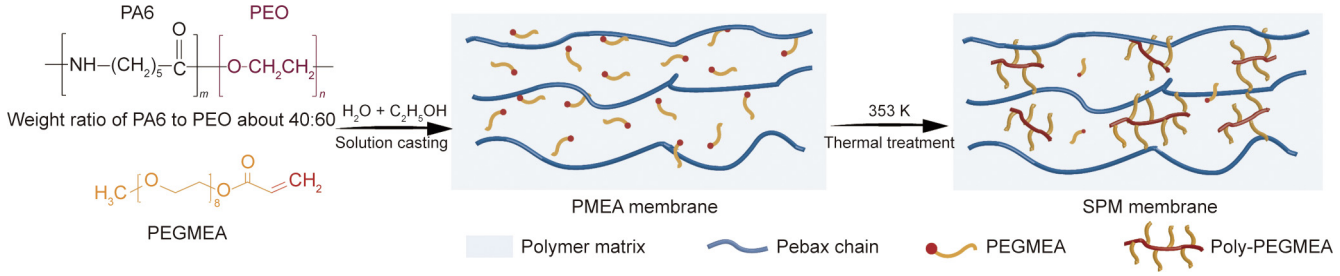

Fig. 1. Schematic illustration of the synthesis process of SPM membranes.

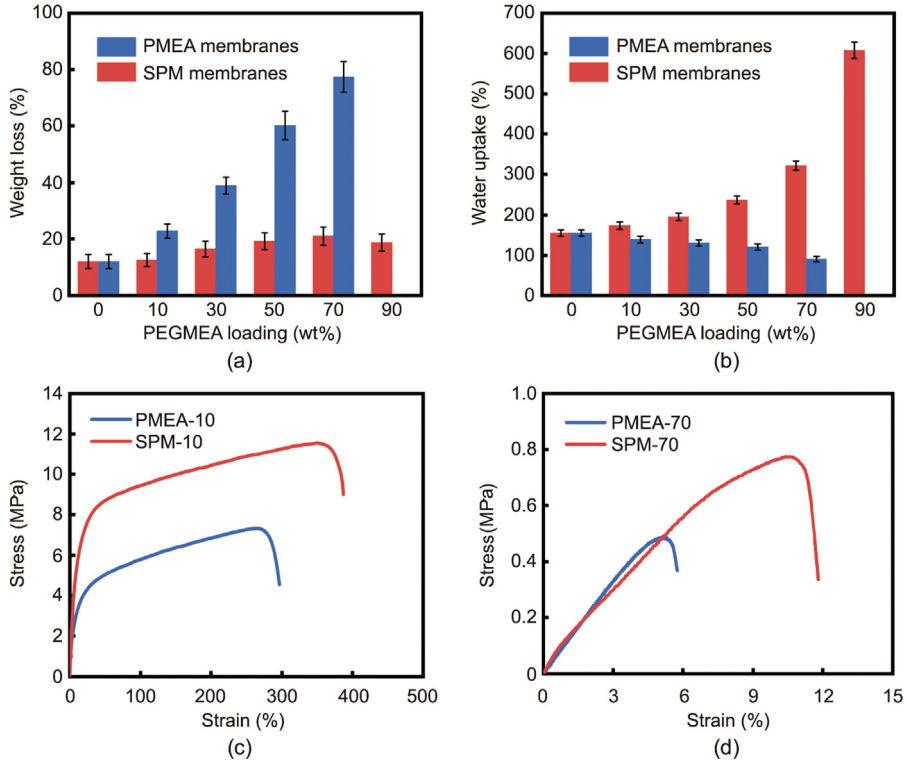

Fig. 2. Comparison of macroscopic properties between PMEA and SPM membranes. (a) Weight loss and (b) water uptake of membranes after water soaking for 72 h. (c, d) Stress–strain curves.

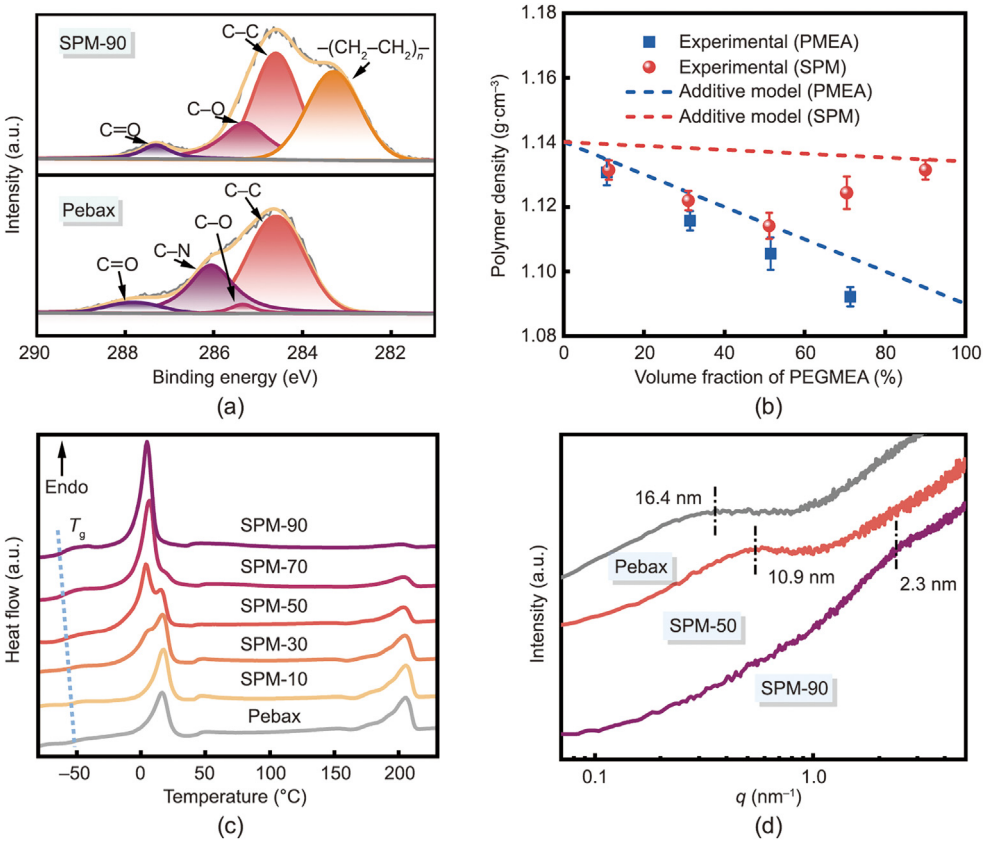

Fig. 3. Structural characterization of membranes. (a) C 1s spectra. (b) Density. (c) DSC thermograms. (d) SAXS patterns, where the q represents for the scattering vector.

In SPM membranes, poly-PEGMEA might be inserted between the PEO and PA6 chains, and the methoxy end group would prohibit any hydrogen bonding interactions to prevent the assembly of PEO and PA6 chains. Therefore, the resulting hybrid polymer has a large intermolecular space for micro-Brownian motion. This speculation is also supported by the decrease in the glass transition temperature, which will be discussed in the following section.

Thermal properties of SPM membranes were investigated using DSC (Fig. 3(c)). There are two distinct endothermic peaks at 16.5 and 205.5 °C, which correspond to the melting points of the PEO and PA6 segments, respectively, indicating microphase separation in the Pebax membrane. The degree of crystallinity (X_C) can be obtained using the melting enthalpy (Table 1) [20]. The X_C of PEO increases with the increase in PEGMEA loading (higher EO amounts). On the contrary, for the PA6 phase, the low molecular weight PEGMEA deteriorates the crystal structure with small and imperfect crystallites, which lead to a decreased melting temperature (T_m) and X_C. Although the crystallinity of the PEO phase gradually increases with the addition of PEGMEA, T_m decreases from 16.5 to 4.7 °C, indicating that the PEO phase is in the molten state under conventional operating temperature conditions. Therefore, the amorphous proportion in the blend polymer increases. Besides, the T_g of SPM membranes decreases progressively from −49.1 to −58.5 °C with increased loading. This is because PEGMEA acts as a plasticizer for the Pebax matrix, which can reinforce chain mobility, as discussed above. The change in T_g can be associated with the FFV of the polymer [36]. The FFV increases with a reduction in the T_g for rubbery polymers. Therefore, it is possible that gas diffusivity and solubility improve as the amorphous proportion and free volume increases. Furthermore, all SPM membranes remained stable up to 300 °C, according to the TGA results (Fig. S6 in Appendix A), suggesting their suitability for high-temperature applications.

SAXS is an effective method to investigate the microstructure of polymers and can directly reflect the microphase separation of block copolymers. All SAXS curves (Fig. 3(d)) exhibit a broad peak, indicating that the membranes form microdomains with a short-range order. Pristine Pebax exhibits a micro-phase separation structure with a nanodomain size of 16.4 nm, according to the Bragg relation [37]. As the PEGMEA content increased, a gradual rightward shift of the peak position was observed, and the intensity gradually decreased, suggesting a breakdown of the microphase separation structure. Similarly, according to the WAXD curves (Fig. S7 in Appendix A), the intensity of the PA6 peak at 2θ = 24° gradually decreased. This suggests that poly-PEGMEA adversely affects the crystallization behavior of the PA6 phase, leading to reduced crystallinity and an increase in the amorphous domain in the SPM membrane, thereby corroborating the DSC and SAXS results.

3.3. Gas separation performance

Figs. 4(a) and (b) show the pure gas separation performances of the Pebax and SPM membranes at 3.5 bar and 35 °C. As the PEGMEA content increased from 0 to 90%, the permeability of all gases improved significantly. Specifically, the CO_2 permeability increased considerably by 568% from 100.6 Barrer (1 Barrer = 10^{-10} $cm^3(STP)\cdot cm\cdot(cm^2\cdot s\cdot cmHg)^{-1}$ = 7.5006 × 10^{-18} $m^3\cdot m\cdot(m^2\cdot s\cdot Pa)^{-1}$) for pristine Pebax to 672.4 Barrer for the SPM-90 membrane. Considering this together with the DSC data, the increase in gas permeability is largely due to the optimization of the free volume. First, the introduction of PEGMEA alters the stacking of the original Pebax chains and enhances their motility. Second, the free unreacted –OCH_3 terminal group acts as a spacer to further expand the free volume fraction of the membrane. Moreover, PEGMEA has a higher EO content than Pebax, which allows an intensive CO_2 solution process. The CO_2/N_2 selectivity marginally increased from 44 to 47, and the CO_2/H_2 selectivity improved by 51.8% (to 12.9) with the PEGMEA incorporation.

To clarify the reason behind the change in the separation performance after the PEGMEA embedment, gas solubility and diffusivity were studied using the time-lag method. Normalized coefficients were employed to study the effect of the PEGMEA content on the gas transport properties (Figs. 4(c) and (d); Table S2 in Appendix A). The solubility and diffusivity of all gases showed an increasing trend. Crystalline polymers usually exhibit low gas solubility owing to their regular and tightly packed structures [38]. However, the introduction of PEGMEA reduces the proportion of crystalline phases in the membrane and increases the amorphous phase, thereby improving the gas solubility of the membrane. Moreover, owing to the dipolar–quadrupole interaction, the increase in EO units in the membrane improves the specific solubility of the membrane for CO_2, ultimately enabling an overall increase in the solubility selectivity. Gas diffusivity is often related to the polymer FFV. Therefore, gas diffusivities increase with increasing PEGMEA content. Notably, when the FFV of the membrane increases, gas molecules with larger kinetic diameters are more influential, and therefore, the gas diffusion coefficient increases in the sequence of N_2 > CO_2 > H_2. This results in an increase and a decrease in CO_2/H_2 and CO_2/N_2 diffusivity selectivities, respectively. Consequently, CO_2/H_2 selectivity significantly increases, which suggests that this novel membrane is suitable for CO_2/light gas separation.

Simultaneously, the Maxwell model was used to estimate gas permeation in SPM membranes, which has been proven to be valid over the entire composition range for the dispersion of isometric particles. The permeability of the composite membrane can be described using the following equation:

$$P_b = P_c \frac{P_d + 2P_c - 2\phi(P_c - P_d)}{P_d + 2P_c - \phi(P_c - P_d)} \quad (4)$$

where P_b, P_c, and P_d are gas permeabilities of the composite material, continuous phase, and discontinuous phase, respectively. The volume fraction of the discontinuous phase is represented by ϕ. Herein, P_c and P_d are the intrinsic permeabilities of Pebax and poly-PEGMEA, respectively. The value for P_d was obtained from the Freeman's study [35]. The experimental and theoretical values

Table 1
Thermal properties of the Pebax and SPM membranes.

Sample	T_g (°C)	PEO phase			PA6 phase	
		T_{m1} (°C)	T_{m2} (°C)	X_C (%)	T_m (°C)	X_C (%)
Pebax	−49.1	—	16.5	27.3	205.5	37.7
SPM-10	−50.6	—	17.4	28.9	205.7	31.8
SPM-30	−53.0	5.2	16.9	30.1	204.9	30.7
SPM-50	−55.1	4.1	15.5	34.6	203.8	27.0
SPM-70	−56.7	4.7	—	37.7	203.8	25.3
SPM-90	−58.5	4.7	—	38.4	201.0	17.0

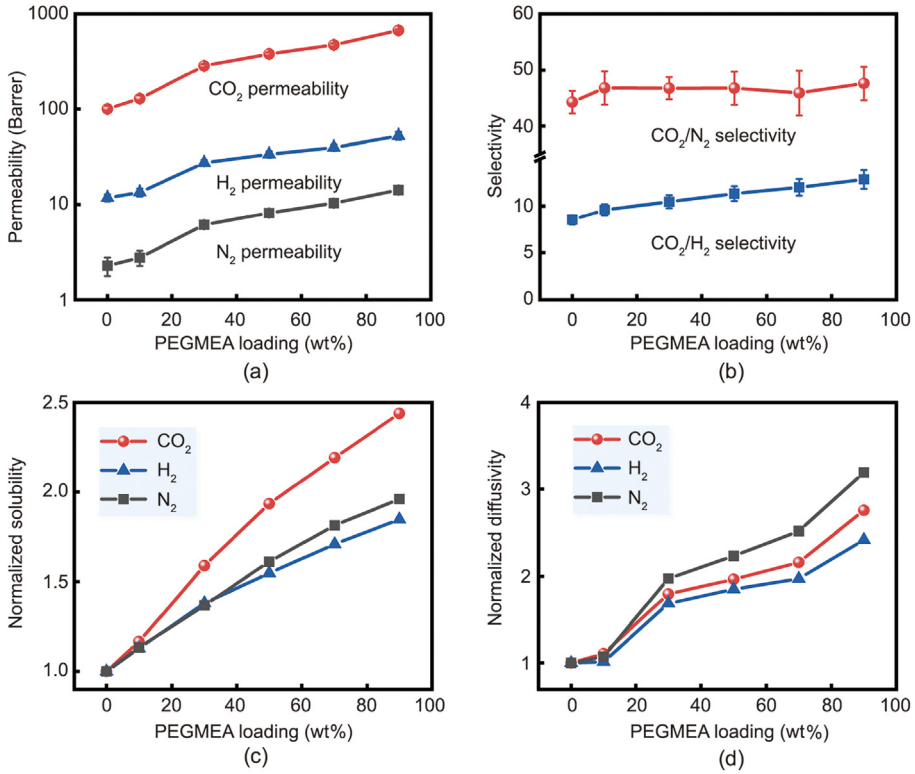

Fig. 4. (a) Gas permeability (1 Barrer = 7.5006 × 10^{-18} $m^3 \cdot m \cdot (m^2 \cdot s \cdot Pa)^{-1}$), (b) selectivity, (c) normalized solubility, and (d) normalized diffusivity of Pebax and SPM membranes at 3.5 bar and 35 °C.

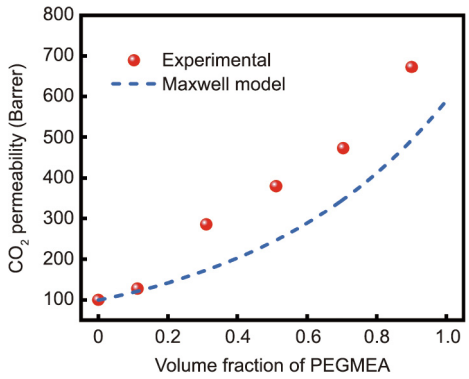

Fig. 5. Experimental values and Maxwell model estimation of the variation of CO_2 permeability with different PEGMEA volume fractions.

of gas permeability in SPM membranes are shown in Fig. 5, and a distinct deviation between the experimental and Maxwell model values is observed, which may be because of the alteration of the structure of the Pebax matrix by the introduction of PEGMEA. Although this model provides only a crude estimation of the connection between the permeability and composition of polymer blends, the results support the conclusion that the significant enhancement of gas permeability is related to the membrane FFV changes owing to the addition of PEGMEA.

A pressure test was conducted to further investigate the operational stability of the membranes. As shown in Fig. 6(a), both CO_2 permeability and CO_2/N_2 selectivity of SPM-90 membrane gradually increase as the feed pressure increases from 3.5 to 20 bar. The increased CO_2 permeability is mainly due to the CO_2 solubility because high pressure can facilitate gas dissolution in a polymer. Therefore, a large amount of CO_2 in the membrane promotes the motility of polymer chains, thereby increasing the FFV, which is known as the plasticization effect. In contrast, N_2 permeability decreases monotonically (Fig. S8 in Appendix A) because the N_2 solubility is low. Plasticization effect does not occur, and membrane compression at high feed pressures leads to FFV loss [28]. Consequently, these two separate trends jointly promoted the enhancement of the CO_2/N_2 selectivity. For the PMEA-70 membrane, CO_2 permeability decreased from 916.1 to 710.3 Barrer as the pressure increased. The reason for this can be inferred from Fig. S9 in Appendix A. The linear PEGMEA was forced out of the membrane after the pressure test, which has also been reported by Shin et al. and termed as the "leaching out" effect [39]. Consequently, when gas pressure decreased from 20 to 3.5 bar, the separation performance of the SPM-90 membrane is reversible (644.7 Barrer), while the PMEA-70 membrane showed a significant decrease in performance to 449.3 Barrer owing to the PEGMEA loss. The enhanced performance of the SPM membrane in the pressure test emphasizes the importance of the self-polymerized structure, which allows a high PEGMEA loading while maintaining superior structural stability.

The effects of the operating temperatures on the CO_2 permeability and CO_2/N_2 selectivity are shown in Fig. 6(b) and Fig. S10 in Appendix A. The CO_2 permeability is notably improved as the temperature increases, owing to the enhancement in the average kinetic energy and mobility of the polymer chains [40]. However, a decreasing trend was observed for CO_2/N_2 selectivity, which corresponds to the decreased CO_2 solubility, as previously reported [41]. In addition, the activation energy is often used to interpret the temperature dependence of the membrane separation performance, which can be described using the Arrhenius equation:

$$P_A = P_{A0} e^{\left(\frac{-E_p}{RT}\right)} \quad (5)$$

where P_A is the permeability (Barrer); P_{A0} represents the pre-exponential factor; R is the universal gas constant ($J \cdot mol^{-1} \cdot K^{-1}$); T

is the absolute temperature (K), and E_P is the activation energy (kJ·mol^{-1}). The calculated results are presented in Table S3 in Appendix A. Both the CO_2 and N_2 apparent activation energy values (from 30 to 55 °C) of SPM-90 are smaller than those of pristine Pebax membranes, revealing the lower gas permeation energy barrier for the SPM membrane.

The long-term stability of the SPM-90 membrane for CO_2/N_2 separation was investigated at 3.5 bar and 35 °C for 120 h. As shown in Fig. 6(c), the CO_2 permeability slightly decreased in the first 24 h, which may be due to the loss of free PEGMEA. However, the value was finally stabilized at 650 Barrer after 120 h. Therefore, this minor change does not have a significant effect on the membrane selectivity, demonstrating the outstanding long-term stability of our SPM membranes.

Figs. 6(d) and (e) compare the CO_2/N_2 and CO_2/H_2 separation performances of the SPM membranes with Robeson's upper-bound line [47]. As the PEGMEA content increased, the separation performance of the SPM membranes approached the upper limit, while the performance of the SPM-90 membrane surpassed the upper-bound limit for the CO_2/N_2 gas pair. As for CO_2/H_2 separation, our study demonstrated a simultaneous increase in both permeability and selectivity, thereby mitigating the well-known "trade-off" effect. Moreover, a higher test pressure increased the membrane performance to a higher level, which is beneficial for the practical application of CO_2-philic membranes.

Finally, the comprehensive performance of our SPM membranes was competitive with that of other Pebax-based polymer blending membranes (Table 2) [19,20,24,32,39,42-46], outlining the nature of the self-polymerized structure. The SPM additive content is higher than the previously reported values and can reach as high as 90 wt%, benefitting from sufficient entanglement between poly-PEGMEA and Pebax chains. Meanwhile, the large number of EO units increases the affinity of the membrane for CO_2 molecules and enables a superior separation performance compared with other polymer blending membranes especially driven by the plasticizing effect. Therefore, we believe that our self-polymerization-confined all-polymeric

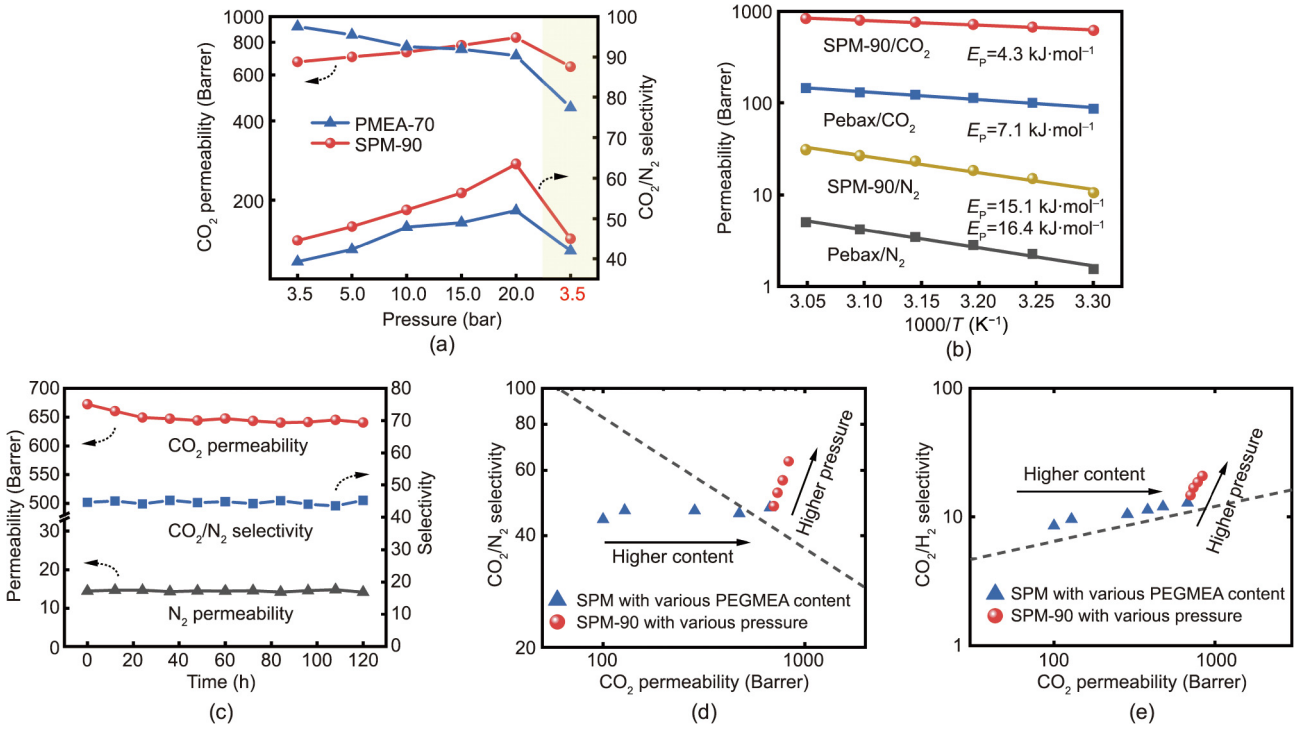

Fig. 6. Effect of (a) feed pressure and (b) temperature on the separation performance. (c) Long-term stability of SPM-90 membrane at 3.5 bar and 35 °C for 120 h. (d, e) Comparison of the separation performance of SPM membranes with an upper-bound line.

Table 2
Performance comparison of composite Pebax membranes based on polymer blends.

Additive	Content (wt%)	Test condition (bar·°C^{-1})	$P(CO_2)$ (Barrer)	CO_2/H_2	CO_2/N_2	Reference
PBE	5	1/35	175.3	—	48.2	[19]
PGP-POEM	40	1/35	236.6	—	38.8	[20]
PEGDME	50	0.3/30	606	15.2	43	[24]
PEG400/POP	1.5/1	1/30	392	—	112	[32]
PEG-MEA/GO	50/0.3	1/35	595	—	55.8	[39]
PEG200	50	0.6/30	151	10.8	47	[42]
PTMEG	80	4/25	245	12	62	[43]
PDMS-PEG	50	4/35	532	10.6	36.1	[44]
L-61	50	5/25	304	—	26	[45]
PDMS-g-POEM	50	1/35	475	—	41.7	[46]
SPM	90	3.5/35	672.4	12.9	47.0	This study
SPM	90	20/35	832	20.8	63.5	This study

PBE: poly(2-[3-(2H-benzotriazol-2-yl)-4hydroxyphenyl]ethyl methacrylate)-graft-poly(oxyethylene methacrylate); PGP: poly(glycidyl methacrylate-g-polypropylene glycol); POEM: poly(oxyethylene methacrylate); PEGDME: polyethylene glycol dimethyl ether; POP: porous organic polymer; GO: graphene oxide; PTMEG: poly(tetramethylene ether) glycol; PDMS: polydimethylsiloxane; L-61: Pluronics L-61; g: graft.

CO_2-philic membrane is suitable for commercialization, owing to its facile synthesis strategy and excellent performance.

4. Conclusions

In summary, a self-polymerization-confined membrane with ultra-stability was successfully fabricated via a facile one-step method. The resulting membranes exhibited superior CO_2/light gas separation performance compared with the conventional membranes, owing to the high content of the amorphous PEO phase. The robust structure, which was derived from the intricate entanglements between poly-PEGMEA and Pebax chains, endows the membrane with excellent mechanical properties and enables an extremely high loading of PEGMEA (up to 90 wt%). Therefore, the separation performance easily surpasses the conventional upper-bound limit. Moreover, good structural stability allows further increases in CO_2 permeability (up to 832 Barrer), CO_2/N_2 selectivity (up to 63.5), and CO_2/H_2 selectivity (up to 20.8) at a high feed pressure of 20 bar. Finally, during the long-term stability tests, the gas separation performance exhibited negligible attenuation for up to 120 h. The typical as-developed self-polymerized structure will aid the progress of polymer workability toward the practical application of membranes for addressing various energy and environmental issues.

Acknowledgment

This work was supported by the National Natural Science Foundation of China (21878062, 21878062, and 22111530113), the Natural Science Foundation of Heilongjiang Province for Distinguished Young Scholars (JQ2020B001), Heilongjiang Touyan Team (HITTY-20190033), Fundamental Research Funds for the Central Universities, and State Key Laboratory of Urban Water Resource and Environment (Harbin Institute of Technology) (2020DX02).

Compliance with ethics guidelines

Bin Zhu, Shanshan He, Yadong Wu, Songwei Li, and Lu Shao declare that they have no conflict of interest or financial conflicts to disclose.

Appendix A. Supplementary data

Supplementary data to this article can be found online at https://doi.org/10.1016/j.eng.2022.03.016.

References

[1] Seneviratne SI, Donat MG, Pitman AJ, Knutti R, Wilby RL. Allowable CO_2 emissions based on regional and impact-related climate targets. Nature 2016;529(7587):477–83.
[2] Chen X, Fan Y, Wu L, Zhang L, Guan D, Ma C, et al. Ultra-selective molecular-sieving gas separation membranes enabled by multi-covalent-crosslinking of microporous polymer blends. Nat Commun 2021;12(1):6140.
[3] He S, Zhu B, Jiang X, Han G, Li S, Lau CH, et al. Symbiosis-inspired *de novo* synthesis of ultrahigh MOF growth mixed matrix membranes for sustainable carbon capture. Proc Natl Acad Sci USA 2022;119(1):e2114964119.
[4] Pulselli RM, Broersma S, Martin CL, Keeffe G, Bastianoni S, van den Dobbelsteen A. Future city visions. The energy transition towards carbon-neutrality: lessons learned from the case of Roeselare, Belgium. Renew Sustain Energy Rev 2021;137:110612.
[5] He X. Polyvinylamine-based facilitated transport membranes for post-combustion CO_2 capture: challenges and perspectives from materials to processes. Engineering 2021;7(1):124–31.
[6] Zeng H, He S, Hosseini SS, Zhu B, Shao L. Emerging nanomaterial incorporated membranes for gas separation and pervaporation towards energetic-efficient applications. Adv Membr 2022;2:100015.
[7] Wang Y, Wang X, Guan J, Yang L, Ren Y, Nasir N, et al. 110th anniversary: mixed matrix membranes with fillers of intrinsic nanopores for gas separation. Ind Eng Chem Res 2019;58(19):7706–24.
[8] Liang CZ, Chung TS, Lai JY. A review of polymeric composite membranes for gas separation and energy production. Prog Polym Sci 2019;97:101141.
[9] Han W, Zhang C, Zhao M, Yang F, Yang Y, Weng Y. Post-modification of PIM-1 and simultaneously *in situ* synthesis of porous polymer networks into PIM-1 matrix to enhance CO_2 separation performance. J Membr Sci 2021;636:119544.
[10] Zhu B, Jiang Xu, He S, Yang X, Long J, Zhang Y, et al. Rational design of poly (ethylene oxide) based membranes for sustainable CO_2 capture. J Mater Chem A 2020;8(46):24233–52.
[11] Meshkat S, Kaliaguine S, Rodrigue D. Comparison between ZIF-67 and ZIF-8 in Pebax® MH-1657 mixed matrix membranes for CO_2 separation. Sep Purif Technol 2020;235:116150.
[12] Liu W, Jiang SD, Yan Y, Wang W, Li J, Leng K, et al. A solution-processable and ultra-permeable conjugated microporous thermoset for selective hydrogen separation. Nat Commun 2020;11(1):1633.
[13] Ebadi Amooghin A, Mashhadikhan S, Sanaeepur H, Moghadassi A, Matsuura T, Ramakrishna S. Substantial breakthroughs on function-led design of advanced materials used in mixed matrix membranes (MMMs): a new horizon for efficient CO_2 separation. Prog Mater Sci 2019;102:222–95.
[14] He S, Zhu B, Li S, Zhang Y, Jiang X, Hon Lau C, et al. Recent progress in PIM-1 based membranes for sustainable CO_2 separations: polymer structure manipulation and mixed matrix membrane design. Sep Purif Technol 2022;284:120277.
[15] Shen L, Yi M, Japip S, Han C, Tian L, Lau CH, et al. Breaking through permeability–selectivity trade-off of thin-film composite membranes assisted with crown ethers. AIChE J 2021;67(6):e17173.
[16] Deng J, Dai Z, Hou J, Deng L. Morphologically tunable mof nanosheets in mixed matrix membranes for CO_2 separation. Chem Mater 2020;32 (10):4174–84.
[17] Ma L, Svec F, Lv Y, Tan T. *In situ* bottom-up growth of metal-organic frameworks in a crosslinked poly(ethylene oxide) layer with ultrahigh loading and superior uniform distribution. J Mater Chem A 2019;7(35):20293–301.
[18] Lilleby Helberg RM, Dai Z, Ansaloni L, Deng L. PVA/PVP blend polymer matrix for hosting carriers in facilitated transport membranes: aynergistic enhancement of CO_2 separation performance. Green Energy Environ 2020;5(1):59–68.
[19] Lee JH, Park CH, Jung JP, Kim JH, Kim JH. Dual-phase all-polymeric membranes with graft copolymer filler for CO_2 capture. Chem Eng J 2018;334:939–47.
[20] Kim NU, Park BJ, Park MS, Park JT, Kim JH. Semi-interpenetrating polymer network membranes based on a self-crosslinkable comb copolymer for CO_2 capture. Chem Eng J 2019;360:1468–76.
[21] Yang X, Martinson ABF, Elam JW, Shao L, Darling SB. Water treatment based on atomically engineered materials: atomic layer deposition and beyond. Matter 2021;4(11):3515–48.
[22] Brinkmann T, Lillepärg J, Notzke H, Pohlmann J, Shishatskiy S, Wind J, et al. Development of CO_2 selective poly(ethylene oxide)-based membranes: from laboratory to pilot plant scale. Engineering 2017;3(4):485–93.
[23] Lau CH, Liu S, Paul DR, Xia J, Jean YC, Chen H, et al. Silica nanohybrid membranes with high CO_2 affinity for green hydrogen purification. Adv Energy Mater 2011;1(4):634–42.
[24] Yave W, Car A, Peinemann KV. Nanostructured membrane material designed for carbon dioxide separation. J Membr Sci 2010;350(1–2):124–9.
[25] Quan S, Tang YP, Wang ZX, Jiang ZX, Wang RG, Liu YY, et al. PEG-imbedded PEO membrane developed by a novel highly efficient strategy toward superior gas transport performance. Macromol Rapid Commun 2015;36(5):490–5.
[26] Li F, Zhang C, Weng Y. Preparation and gas separation properties of triptycene-based microporous polyimide. Macromol Chem Phys 2019;220(10):1900047.
[27] Yan L, Yang X, Zhao Y, Wu Y, Motlhaletsi Moutloali R, Mamba BB, et al. Bio-inspired mineral–hydrogel hybrid coating on hydrophobic pvdf membrane boosting oil/water emulsion separation. Separ Purif Technol 2022;285:120383.
[28] Jiang X, He SS, Li SW, Bai YP, Shao L. Penetrating chains mimicking plant root branching to build mechanically robust, ultra-stable CO_2-philic membranes for superior carbon capture. J Mater Chem A 2019;7(28):16704–11.
[29] Zhang C. Synthesis and characterization of bis(phenyl)fluorene-based cardo polyimide membranes for H_2/CH_4 separation. J Mater Sci 2019;54 (14):10560–9.
[30] Hong H, Gao L, Zheng Y, Xing X, Sun F, Liu T, et al. A path of multi-energy hybrids of concentrating solar energy and carbon fuels for low CO_2 emission. ES Energy Environ 2021:1–7.
[31] Pellessier J, Gang Y, Li Y. A sustainable synthesis of nickel–nitrogen–carbon catalysts for efficient electrochemical CO_2 reduction to CO. ES Mater Manuf 2021;13:66–75.
[32] He R, Cong S, Xu S, Han S, Guo H, Liang Z, et al. CO_2-philic mixed matrix membranes based on low-molecular-weight polyethylene glycol and porous organic polymers. J Membr Sci 2021;624:119081.
[33] Wang W, Sun J, Zhang Y, Zhang Y, Hong G, Moutloali RM, et al. Mussel-inspired tannic acid/polyethyleneimine assembling positively-charged membranes with excellent cation permselectivity. Sci Total Environ 2022;817:153051.
[34] Shi F, Sun J, Wang J, Liu M, Yan Z, Zhu B, et al. Mxene versus graphene oxide: investigation on the effects of 2D nanosheets in mixed matrix membranes for CO_2 separation. J Membr Sci 2021;620:118850.
[35] Lin H, Wagner E, Swinnea J, Freeman B, Pas S, Hill A, et al. Transport and structural characteristics of crosslinked poly(ethylene oxide) rubbers. J Membr Sci 2006;276(1–2):145–61.
[36] Zhang C, Li P. Preparation and gas separation properties of spirobichroman-based polyimides. Macromol Chem Phys 2018;219(16):1800157.

[37] Magana S, Sudre G, Gouanvé F, Cousin F, Espuche E. Influence of the film-forming process on the nanostructuration of Pebax®/1-ethyl-3-methylimidazolium triflate ionic liquid: consequences on the thermal, mechanical, gas, and water transport properties. J Polym Sci, B, Polym Phys 2017;55(10):778–88.
[38] Reijerkerk SR, Wessling M, Nijmeijer K. Pushing the limits of block copolymer membranes for CO_2 separation. J Membr Sci 2011;378(1–2):479–84.
[39] Shin JE, Lee SK, Cho YH, Park HB. Effect of PEG-MEA and graphene oxide additives on the performance of Pebax®1657 mixed matrix membranes for CO_2 separation. J Membr Sci 2019;572:300–8.
[40] Kim JH, Ha SY, Lee YM. Gas permeation of poly(amide-6-*b*-ethylene oxide) copolymer. J Membr Sci 2001;190(2):179–93.
[41] Liu J, Zhang S, Jiang D, Doherty CM, Hill AJ, Cheng C, et al. Highly polar but amorphous polymers with robust membrane CO_2/N_2 separation performance. Joule 2019;3(8):1881–94.
[42] Car A, Stropnik C, Yave W, Peinemann KV. PEG modified poly(amide-*b*-ethylene oxide) membranes for CO_2 separation. J Membr Sci 2008;307(1):88–95.
[43] Rabiee H, Ghadimi A, Abbasi S, Mohammadi T. CO_2 separation performance of poly(ether-*b*-amide6)/PTMEG blended membranes: permeation and sorption properties. Chem Eng Res Des 2015;98:96–106.
[44] Reijerkerk SR, Knoef MH, Nijmeijer K, Wessling M. Poly(ethylene glycol) and poly(dimethyl siloxane): combining their advantages into efficient CO_2 gas separation membranes. J Membr Sci 2010;352(1–2):126–35.
[45] Didden J, Thür R, Volodin A, Vankelecom IFJ. Blending PPO-based molecules with Pebax MH 1657 in membranes for gas separation. J Appl Polym Sci 2018;135(27):46433.
[46] Kim SJ, Jeon H, Kim DJ, Kim JH. High-performance polymer membranes with multi-functional amphiphilic micelles for CO_2 capture. Chem Sus Chem 2015;8(22):3783–92.
[47] Robeson LM. The upper bound revisited. J Membr Sci 2008;320(1–2):390–400.